



# High pyroelectric effect in poly(vinylidene fluoride) composites cooperated with diamond nanoparticles

Wenru Li<sup>a,1</sup>, An Zheng<sup>a,1</sup>, Yuli Lin<sup>a</sup>, Pin Liu<sup>a</sup>, Meng Shen<sup>a</sup>, Licheng Zhou<sup>a</sup>, Huan Liu<sup>a</sup>, Jiale Yuan<sup>b</sup>, Shuang Qin<sup>c</sup>, Xu Zhang<sup>c</sup>, Nuo Yang<sup>b</sup>, Shenglin Jiang<sup>a,d,\*</sup>, Guangzu Zhang<sup>a,\*</sup>

<sup>a</sup>School of Optical and Electronic Information, Engineering Research Center for Functional Ceramics MOE and Wuhan National Laboratory for Optoelectronics, Huazhong University of Science and Technology, Wuhan 430074, China

<sup>b</sup>School of Energy and Power Engineering, Huazhong University of Science and Technology Wuhan, Hubei 430074, China

<sup>c</sup>Institute of Fluid Physics, China Academy of Engineering Physics, Mianyang, Sichuan 621900, China

<sup>d</sup>Shenzhen Huazhong University of Science and Technology Research Institute, Shenzhen, Guangdong 518057, China

## ARTICLE INFO

### Article history:

Received 11 December 2019

Received in revised form 31 January 2020

Accepted 16 February 2020

Available online 18 February 2020

### Keywords:

Ferroelectrics

Polymers

PVDF

Diamond nanoparticles

Pyroelectric

Thermal conductivity

## ABSTRACT

In this work, the synthetic diamond nanoparticles are used as the non-ferroelectric fillers to obtain high pyroelectric performance in PVDF composite films. The oxygen-containing groups that inherently exist on the surface of the diamond nanoparticles make more content of PVDF transform from the  $\alpha$ -phase to the  $\beta$ -phase, contributing to the high pyroelectric coefficient. The 0.4 wt% diamond/PVDF film shows the highest pyroelectric coefficient of 870,000  $\mu\text{C}/\text{cm}^2\text{K}$ , which is 3.5 times higher than the pristine PVDF. As a result, the diamond/PVDF films generate higher pyroelectric current and voltage than the pristine PVDF film.

© 2020 Elsevier B.V. All rights reserved.

## 1. Introduction

Pyroelectrics can convert the temperature fluctuation into electric signals and play an essential role in the many advanced electronic devices [1–3]. Poly(vinylidene fluoride) (PVDF) is one of the most widely researched pyroelectrics due to its unique flexible property and easy fabrication [4,5]. However, the pyroelectric coefficient ( $p$ ) of pristine PVDF film is badly inhibited due to the high content of non-ferroelectric  $\alpha$ -phase PVDF [6]. It has been widely studied how to enhance the pyroelectric performances of PVDF by increasing the content of the ferroelectric  $\beta$ -phase. On the one hand, the co-/ter-polymers, such as poly(vinylidene fluoride-tri fluoroethylene) (P(VDF-TrFE)) [7] and poly(vinylidene fluoride-tri fluoroethylene-chloro fluoroethylene) (P(VDF-TrFE-CFE)) [8], are fabricated, which have high content of  $\beta$ -phase due to the unique atomic distribution [9,10]. But their applications are limited to

the high prices. On the other hand, other methods that used for producing high  $\beta$ -phase content PVDF for example, the Langmuir-Blodgett (LB) method [11], spin coating process [12], preparing composites with ZnO [13] or graphene [14], poling with DC magnetic fields [15], mechanical stretching [16], and hot pressing [17], also attract a lot of attention (Supplementary Note S1).

Herein, the synthetic diamond nanoparticles are used as the non-ferroelectric fillers to enhance the pyroelectric performances of PVDF films through the solution casting method. Compared with the well-known processes, such as the Langmuir-Blodgett method and the spin coating approach, the solution casting method is more suitable for preparing homogenous PVDF composite films with large size and high quality. The synthetic diamond nanoparticles with plentiful oxygen containing groups on its surfaces could transform the  $\alpha$ -phase of PVDF into  $\beta$ -phase. The 0.4 wt% diamond/PVDF film shows a high  $p$  of 870,000  $\mu\text{C}/\text{cm}^2\text{K}$ , which is  $\sim 3$  times higher than the pristine PVDF. Moreover, the diamond with the stable crystal structure, high thermal conductivity ( $k$ ), and low dielectric constant ( $\epsilon'$ ) shows great potential in promoting the dielectric and ferroelectric properties of PVDF film. Compared with the previous works (Table S2), the diamond nanoparticles are demonstrated to be more effective to improve the comprehensive performance of the PVDF polymer.

\* Corresponding authors at: School of Optical and Electronic Information, Engineering Research Center for Functional Ceramics MOE and Wuhan National Laboratory for Optoelectronics, Huazhong University of Science and Technology, Wuhan 430074, China.

E-mail addresses: [jsl@hust.edu.cn](mailto:jsl@hust.edu.cn) (S. Jiang), [zhanggz@hust.edu.cn](mailto:zhanggz@hust.edu.cn) (G. Zhang).

<sup>1</sup> These authors contributed equally to this work.

## 2. Experiment

The PVDF powder (Solef, 6020) and diamond powders (Henan ZhenZuan Abrasive Mould, W1) were dissolved into N, N-dimethylformamide (DMF, Sinopharm, MW73.09) to form a homogeneous solution. After stirring, the mixing solution was dropped onto the glass plate to cast a uniform film. The films were heated at 50 °C for 24 h to drive out the solvent and annealed at 75 °C for another 24 h to increase the crystallinity (Fig. 1a). The fabrication details are described in the [Supplementary Material](#).

The mechanical, morphology, and phase characters of films were analyzed by mechanical-test-machine, SEM, XRD, and FTIR. The  $p$  and polarization–electric field ( $P$ - $E$ ) hysteresis loops were tested by pyroelectric parameter tracer and Sawyer-Tower circuit (PolyK Technologies). The  $\epsilon'$  and dielectric loss ( $\tan\delta$ ) as functions of the frequency were measured by a precision impedance analyzer (Wayne Kerr 6500B). The  $k$  of PVDF films were characterized by a system named  $3\omega$  Setup that set up by Cahill *et al.* [18].

## 3. Results and discussion

Fig. 1b is the SEM picture of diamond nanoparticles showing the grain diameter varying from 300 nm to 600 nm. Compared with

the pristine PVDF, the film with 0.4 wt% diamond has a coarse surface, indicating the diamond nanoparticles are homogeneously mixed into the matrix of PVDF (Fig. 1c and d). The enhanced tensile strength and Young's modulus of diamond/PVDF films prove the fact that there is a strong reaction happened between the PVDF matrix and diamond nanoparticles (Fig. 1e).

The surface functional groups of diamond nanoparticles are characterized by FTIR (Fig. S1a). As shown in Fig. S1a, the absorption peaks at  $3430\text{ cm}^{-1}$  and  $1630\text{ cm}^{-1}$  generate by the stretching vibrations of  $-\text{OH}$  and  $-\text{C}-\text{OH}$  [19], and the prominent absorption peak at  $1381\text{ cm}^{-1}$  is attributed to the  $-\text{OH}$  vibration in carboxyl groups [20]. After mixing with PVDF, the hydrogen bonds would be formed between the  $-\text{CF}_2$  of PVDF and the oxygen-containing groups of the diamond, which makes the PVDF transformed from  $\alpha$ -phase to  $\beta$ -phase [21]. The characteristic absorption peak of  $\alpha$ -phase (at  $763\text{ cm}^{-1}$ ) decreased and the counterpart of  $\beta$ -phase (at  $840\text{ cm}^{-1}$ ) increased gradually (Fig. S1b) [22]. The relative content of  $\beta$ -phase is calculated according to FTIR and summarized in Table S1, which illustrates that the 0.4 wt% diamond/PVDF has the highest  $\beta$ -phase content of 78.7%, while it is 68.9% for the pristine PVDF. The XRD pattern (Fig. S1c) of diamond nanoparticles have peaks at  $44^\circ$  and  $75^\circ$  matching well with the (1 1 1) and (2 2 0) planes of cubic system diamond. Fig. S1d is XRD patterns of the

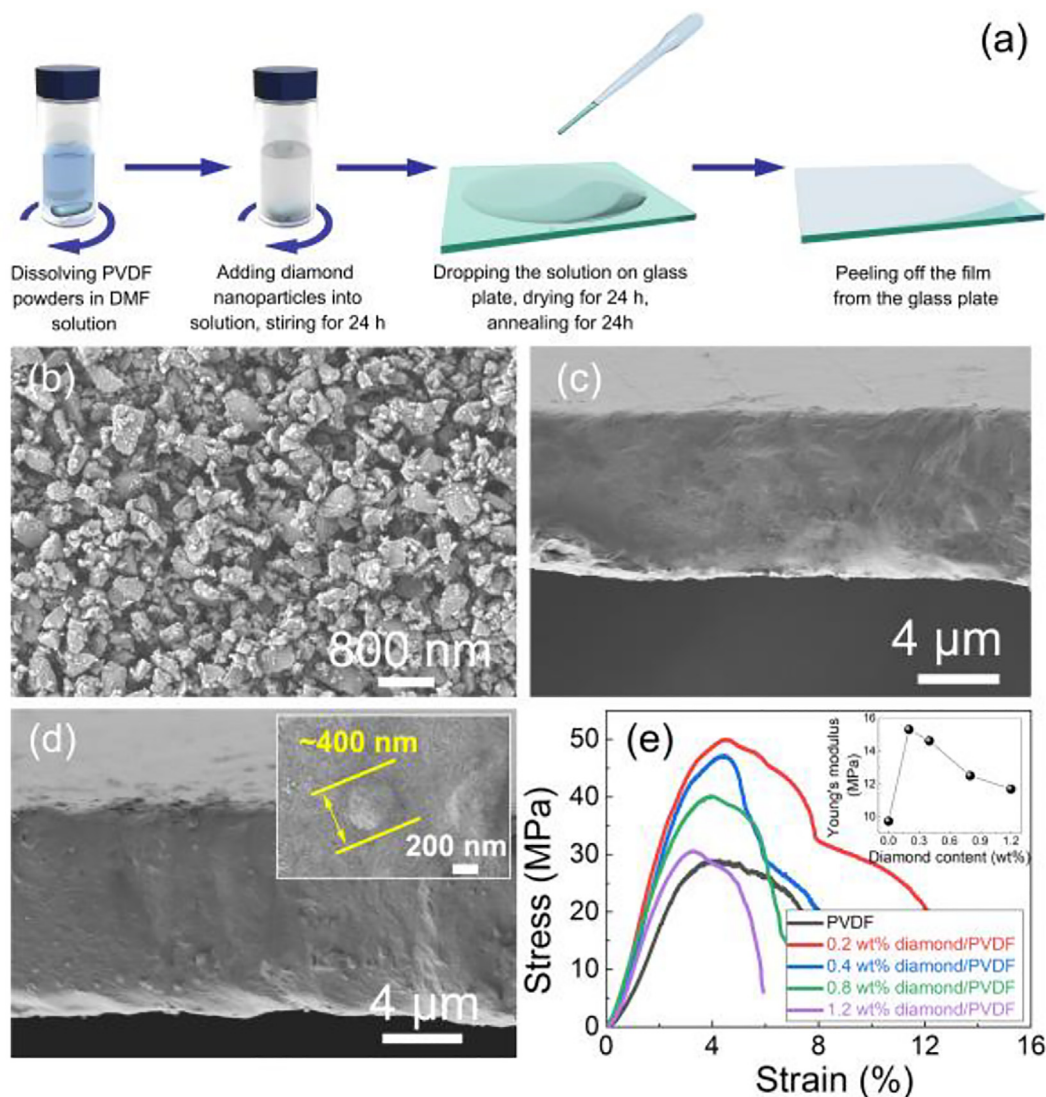


Fig. 1. (a) Fabrication process of diamond/PVDF films. (b) SEM graph of diamond nanoparticles. Cross-section SEM images of (c) pristine PVDF film and (d) 0.4 wt% diamond/PVDF film. (e) Tensile stress-strain properties of diamond/PVDF films with different filling ratios of diamond nanoparticles. Inset pattern is Young's modulus of the films.

pristine and composite PVDF films. The peaks at 19.91° and 20.91° ascribe to the  $\alpha$ - and  $\beta$ -phases of PVDF, respectively.

The pyroelectric curves rise gradually with the increasing temperature (Fig. 2a). The 0.4 wt% diamond/PVDF film has the highest  $p$  that is 870,000  $\mu\text{C}/\text{cm}^2\text{K}$  at 50 °C, which is 3.5 times higher compared to the pristine PVDF. By comparison, the  $p$  of diamond/PVDF film is obviously higher than that of the other PVDF composites mixed with ferroelectric fillers (Table S1). In addition, the  $k$  of 1.2 wt% diamond/PVDF film reaches up to 0.54 W/mK, while that is 0.21 W/mK for the pristine PVDF (Fig. S2a). The enhanced  $k$  can effectively accelerate the thermal transfer rate in composite PVDF films (Fig. S2b) and enhance the pyroelectric voltage and current responses.

The pyroelectric current ( $i_p = p \text{ A } dT/dt$ ) and voltage ( $v_p = p \text{ d } \epsilon' \epsilon_0 \Delta T$ ) were tested and shown in the Fig. 2c-d. A is the area

size of the electrode,  $d$  is the thickness of the film, and  $\epsilon_0$  is the vacuum dielectric constant [23]. It can be found from the formula that the value of  $i_p$  is not only related to the  $p$ , but also depends on the changing rate of temperature (i.e.  $dT/dt$ ). Large  $p$  and  $dT/dt$  are realized in diamond/PVDF films thanks to the high content of  $\beta$ -phase PVDF and the enhanced  $k$  of films. In this experiment, we measure the periodic pyroelectric currents and voltages of the pristine and composite PVDF films at around 40 °C with a small temperature fluctuation ( $\Delta T = \sim 1.2$  °C) (Fig. 2b). Making use of the enhanced  $p$  and  $k$ , the pyroelectric output signals of composite PVDF films are higher than those of the pristine one. As shown in Fig. 3, the diamond nanoparticles also promote the dielectric and ferroelectric performances of PVDF film.

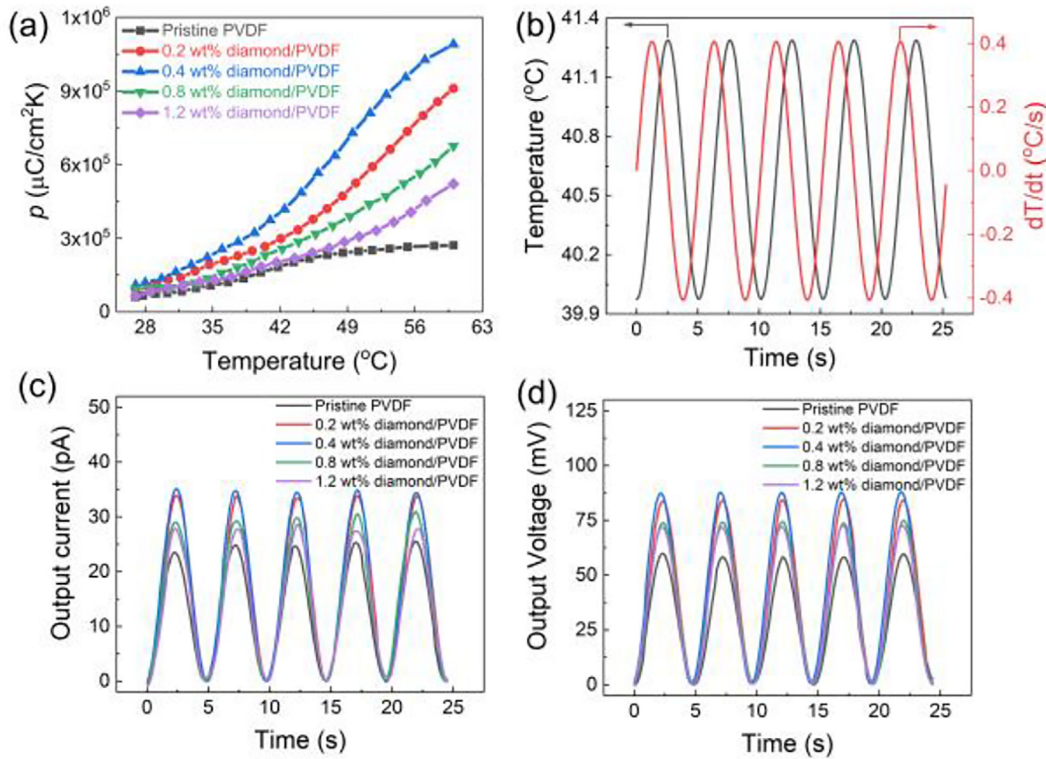


Fig. 2. (a) The  $p$  of the pristine and composite PVDF films. (b) The temperature–time curves. (c) and (d) The output currents and voltages of the pristine and composite PVDF films.

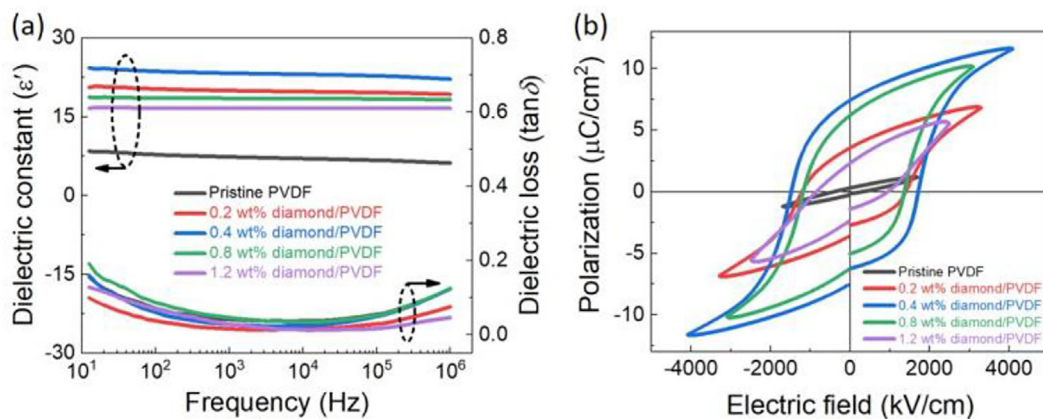


Fig. 3. (a) The  $\epsilon'$  and  $\tan\delta$  of the pristine and composite PVDF films as a function of frequency. (b) The P-E loops of the pristine and composite PVDF films.

#### 4. Conclusion

The synthesized diamond nanoparticles have plenty of oxygen-containing groups on their surface, which can effectively promote the transformation of PVDF from the  $\alpha$ -phase to the  $\beta$ -phase. The high  $\beta$ -phase content raises the  $p$  of diamond/PVDF films to 870,000  $\mu\text{C}/\text{cm}^2\text{K}$ , which is 3.5 times higher than that of pristine PVDF. Moreover, the  $k$  of composite films is significantly enhanced, which helps to generate high pyroelectric signals. In conclusion, the comprehensive performances of the PVDF have been effectively improved by filling non-ferroelectric diamond nanoparticles, and the ferroelectric and pyroelectric properties of the diamond/PVDF composites are demonstrated to be superior to those of typical composites listed in Table S2.

#### Declaration of Competing Interest

The authors declare that they have no known competing financial interests or personal relationships that could have appeared to influence the work reported in this paper.

#### Acknowledgements

This research was supported by the National Natural Science Foundation of China (51972126, 61675076, 51772108 and 51972125), Natural Science Foundation of Hubei Province (2018CFB427), the Fund from Science, Technology and Innovation Commission of Shenzhen Municipality (JCYJ20180507182248925), the Fundamental Research Funds for the Central Universities (2019kfyRCPY126 and 2018KFYXJJ052) and Innovation Fund of WNLO, and Basic Science and Technology Project (JSZL2016212C001). We acknowledge the support from the Analytical and Testing Center, Huazhong University of Science and Technology.

#### Appendix A. Supplementary data

Supplementary data to this article can be found online at <https://doi.org/10.1016/j.matlet.2020.127514>.

#### References

- [1] G.Z. Zhang, P. Zhao, X.S. Zhang, K. Han, T.K. Zhao, Y. Zhang, C.K. Jeong, S.L. Jiang, S.L. Zhang, Q. Wang, *Energy Environ. Sci.* 11 (8) (2018) 2046–2056.
- [2] G.Z. Zhang, S.L. Jiang, Y.Y. Zhang, T.T. Xie, *Curr. Appl. Phys.* 9 (2009) 1434.
- [3] Y.K. Zeng, F. Yao, G.Z. Zhang, S.S. Liu, S.L. Jiang, Y. Yu, J.G. He, L. Zhang, J.Q. Yi, *Ceram. Int.* 39 (2013) 3709.
- [4] H.S. Nalwa, M. Dekker, *New York*, (1995)
- [5] A.J. Lovinger, *Science* 220 (1983) 4602.
- [6] B. Jaleh, S. Sodagar, A. Momeni, A. Jabbari, *Mater. Res. Express* 3 (8) (2016) 085028.
- [7] J.L. Wang, B.L. Liu, X.L. Zhao, B.B. Tian, Y.H. Zou, S. Sun, H. Shen, J.L. Sun, X.J. Meng, J.H. Chu, *Appl. Phys. Lett.* 104 (2014) 182907.
- [8] H.M. Bao, J.F. Song, J. Zhang, Q.D. Shen, C.Z. Yang, Q.M. Zhang, *Macromolecules* 40 (7) (2007) 2371–2379.
- [9] M. Wojtaś, D.V. Karpinsky, M.V. Silibin, S.A. Gavrilov, A.V. Sypa, K.N. Nekludov, S.V. Dubkov, *Polym. Test.* 71 (2018) 296–300.
- [10] M. Wojtas, D.V. Karpinsky, M.V. Silibin, S.A. Gavrilov, A.V. Sypa, K.N. Nekludov, *Polym. Test.* 60 (2017) 326–332.
- [11] V.M. Fridkin, S. Ducharme, *Physics-Uspekhi.* 57 (6) (2014) 597–603.
- [12] S. Palto, L. Blinov, A. Bune, E. Dubovik, V. Fridkin, N. Petukhova, K. Verkhovskaya, S. Yudin, *Ferroelectric Lett.* 9 (1995) 65–68.
- [13] V.S. Bystrov, I.K. Bdikin, M.V. Silibin, X.J. Meng, T. Lin, J.L. Wang, D.V. Karpinsky, A.V. Bystrova, E.V. Paramonova, *Ferroelectrics* 541 (1) (2019) 17–24.
- [14] K.S. Tan, W.C. Gan, T.S. Velayutham, W.H.A. Majid, *Smart Mater. Struct.* 23 (2014) 125006.
- [15] M. Sang, S. Wang, M. Liu, L.F. Bai, W.Q. Jiang, S.H. Xuan, X.L. Gong, *Compos. Sci. Technol.* 165 (2018) 31–38.
- [16] R.X. Bao, M.Y. Li, M. Shen, H. Liu, G.Z. Zhang, Y.K. Zeng, S.L. Jiang, *J. Mater. Sci. Mater. El.* 30 (7) (2019) 6760–6767.
- [17] H.N. Na, Y.P. Zhao, C.G. Zhao, C. Zhao, X.Y. Yuan, *Polym. Eng. Sci.* 48 (5) (2008) 934–940.
- [18] D.G. Cahill, K. Goodson, A. Majumdar, *J. Heat Trans.* 124 (2) (2002) 223–241.
- [19] H. Guo, X. Li, B.A. Li, J.X. Wang, S.C. Wang, *Mater. Design* 114 (2017) 355–363.
- [20] W.S. Tong, Y.H. Zhang, Q. Zhang, X.L. Luan, Y. Duan, S.F. Pan, F.Z. Lv, Q. An, *Carbon* 94 (2015) 590–598.
- [21] C. Yang, S.J. Hao, S.L. Dai, X.Y. Zhang, *Carbon* 117 (2017) 301–312.
- [22] B.C. Luo, X.H. Wang, Y.P. Wang, L.T. Li, *J. Mater. Chem. A* 2 (2) (2014) 510–519.
- [23] C.R. Bowen, J. Taylor, E. LeBoulbar, D. Zabek, A. Chauhan, R. Vaish, *Energy Environ. Sci.* 7 (1) (2014) 25–44.